



## ORIGINAL PAPER

**GEOCHEMICAL STUDY OF THE TONGSHAN INTRUSION IN THE LOWER YANGTZE RIVER METALLOGENIC BELT, CHINA: SIGNIFICANCES OF CU-AU ORE-FORMING**Huangling GU<sup>1,2)</sup>, Zhen LIU<sup>1)</sup>, Lin LI<sup>1)</sup> and Xianchao ZHAO<sup>1)</sup> \*<sup>1)</sup> School of City and Environment, Hunan University of Technology, Zhuzhou 412007, China<sup>2)</sup> School of Metallurgy and Environment, Central South University, Changsha 410083, China

\*Corresponding author's e-mail: 89739097@qq.com

## ARTICLE INFO

**Article history:**

Received 1 July 2022

Accepted 12 December 2022

Available online 31 December 2022

**Keywords:**

Tongshan

Adakite

Late Mesozoic

Partial melting

Subducted oceanic crust

## ABSTRACT

The Tongshan intrusion is located at the Guichi ore cluster field along the Lower Yangtze River metallogenic belt (LYRB) in eastern China. Elemental data and major elements of biotite are reported for Late Mesozoic plutons in the Guichi ore cluster in the Middle-Lower Yangtze River Region, attempting to explain their diagenetic age, petrogenesis, and tectonic implications. The Tongshan intrusion is dated at  $146.3 \pm 3.2$  Ma, with zircon  $\varepsilon_{\text{Hf}}(t)$  average value of  $-5.23$ , illustrating that the Tongshan intrusion could be derived from crust mantle mixing magmatite provenance. The two-stage Hf model ages between 1184–1422 Ma is indicated magma source relationship with those of the Mesoproterozoic basement in south Anhui. The Tongshan intrusion is high-K calc-alkaline, and exhibit adakite-like geochemical feature, such as high  $\text{Al}_2\text{O}_3$ , Sr contents, Sr/Y value, low Y and Yb contents. The geochemical and reexplained published isotopic data indicate that these adakites are most likely from partial melting of subducted oceanic crust, and mixed with enriched lithospheric mantle components in the rising process.

**1. INTRODUCTION**

The Middle-lower Yangtze River region are an important metallogenic belt of copper, gold and polymetallic in eastern China with high research level. Seven ore concentration areas are distinguished from east to west: Edong, Jiurui, Anqing-Guichi, Luzong, Tongling, Ningwu and Ningzhen (Fig. 1a, Chang et al., 1991; Yang and Lee, 2011; Deng et al., 2016). The metallogenic has been dated  $140 \pm 5$  Ma (Zhou et al., 2015; Deng et al., 2016; Wang et al., 2022), and related to the Yanshanian period acid calcium alkaline intrusive (Xie et al., 2018; Hu et al., 2017).

Recently, many researchers have devoted to the tectonic background of the middle-lower Yangtze River metallogenic belt (LYRB). The Magma is mainly composed of three series: high alkali calcium alkali series (Chang et al., 1991), olives-coarse rock series (Chang et al., 1991) and alkaline (type A) granite series (Xu et al., 2021). The tectonic background belongs to continental margin magmatic arc associated with subduction of the ancient Pacific plate (Deng et al., 2004), controlled by the Yangtze river fault zone and the mantle uplift (Chang et al., 1991). The diagenesis and mineralization in the Yangtze river region are in the intraplate magmatism blocks (Chang et al., 1991; Zhou et al., 2015). Skarn gold and related deposits were formed in continental collision extrusion stretch conversion period (Shi et al., 2022).

By contrast, compared with the aforementioned districts, research on the Guichi section in the Anqing-Guichi area has been limited, particularly in terms of geochronology and magma petrogenesis. The absence of such data hinders development of an in-depth understanding of the occurrence and petrogenesis of Mesozoic magmatism in the Anqing-Guichi district and the LYRB as a whole. Tongshan copper deposit is a typical magmatic deposit in the Guichi section of the Anqing-Guichi district, which limited a comprehensive understanding to the magmatic and metallogenic system features of the LYRB (Yang and Lee, 2011; Deng et al., 2016; Wang et al., 2022). Despite these previous studies, the relationship between magmatic rock and mineralization is not clearly described. In this work, the author has tested the main element and trace element content to the Tongshan granodiorite. On the base of the age of the Tongshan granodiorite, copper deposit and the geochemical characteristics, the author has studied the mechanism and tectonic setting of the ore-bearing rock, which enrich the theory of the Yanshanian magmatism and metallogenic model of the LYRB.

**2. REGIONAL GEOLOGICAL SETTING**

The middle-lower Yangtze River locate between north margin of Yangtze Block and south of the North China Craton and Qinling-Dabie Orogen. It extends 400 km from Hubei province in the southwest to

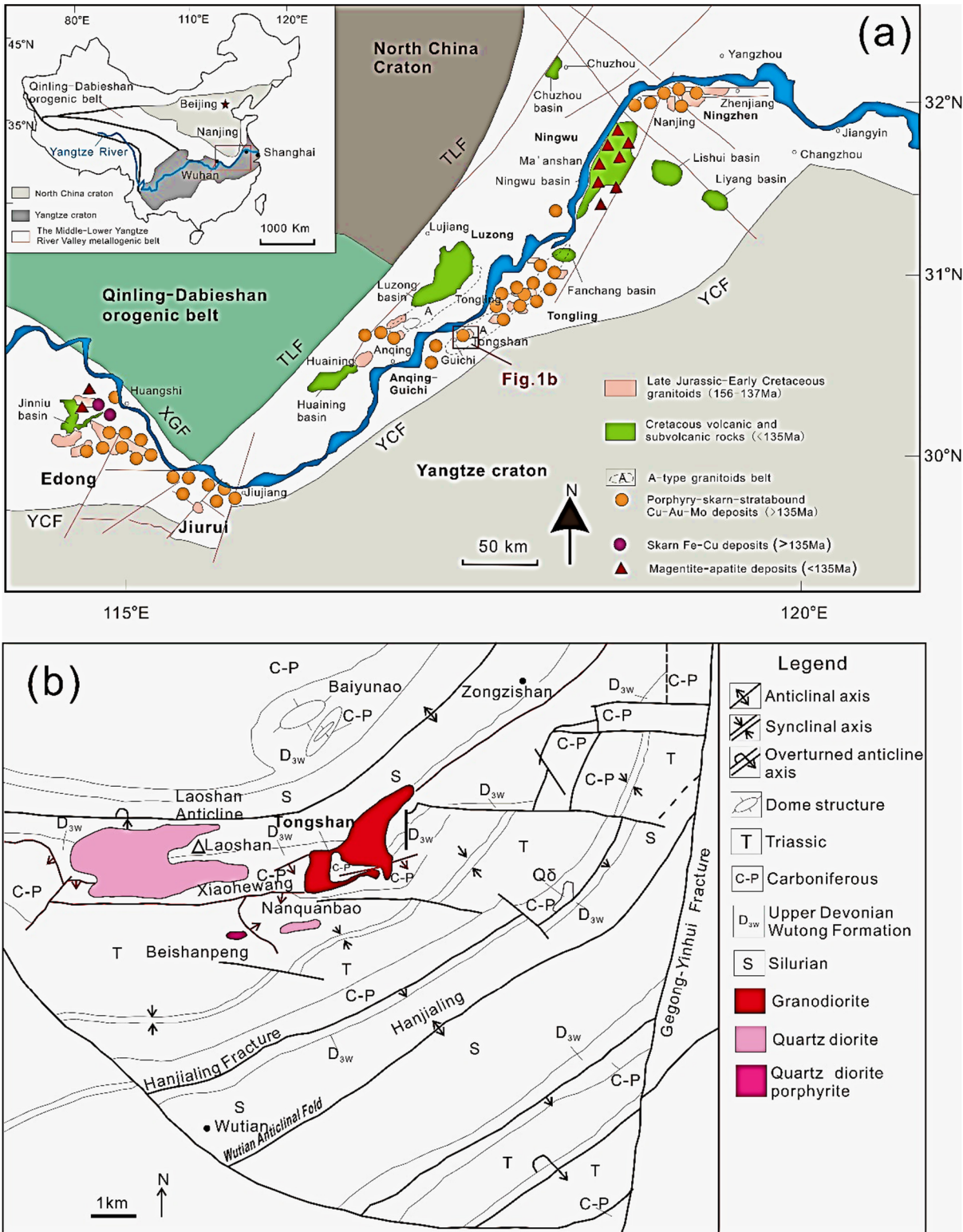


**Fig. 1** (a) Distribution of ore deposits and related granitoids along the LYRB (modified from Mao et al., 2011). (b) Geological map of the Tongshan ore cluster district, Guichi. TLF: Tancheng-Lujiang fault, XGF: Xiangfan-Guangji fault, YCF: Yangxing-Changzhou fault.

Jiangsu province in the northeast. This tectonic evolution has gone through three stages: Basement forming Period in Precambrian, Sinian-Early Permian Sedimentary Period and Triassic Collision Orogenic Period (Chang et al., 1991). And it moved into Pacific

Tectonic Domain with a lot of extensive magmatic activity and crustal extension (Gilder et al., 1991), lead to one of the most important metallogenic belt in Eastern China (Chang et al., 1991). The LYRB is characterized by extensive late Mesozoic magmatism

and ore deposits, and is thus one of the most important regions of giant Mesozoic magmatic activity and mineralization in eastern China (Mao et al., 2011; Sun et al., 2015, 2017; Wang et al., 2020).

The Tongshan copper deposit areas a typical of many ore-bearing plutons in the Anqing-Guichi district of the LYRB is located at the margin of Guichi district (Fig. 1a). The intrusion is structurally located at the bend in the Tongshan arc-shaped structure in the southeastern flank of the Laoshan anticline (Fig. 1b). Strata in the area mainly comprise sedimentary rocks of the Upper Silurian siltstone of the Maoshan Formation and the Lower Triassic limestone of the Biandanshan Formation (Fig. 1b; Zhang et al., 2014). Occurrences of the magmatic rocks are controlled by concealed east-west- and northwest-trending faults, and the shallow sub-surface structure is northeast-trending (Zhang et al., 2013a). At depth, irregular northeast-trending stocks occur and crop out at the surface over an area of approx. 2 km<sup>2</sup>. The surrounding country rocks are Silurian-Devonian clastic sediments and Carboniferous-Permian carbonate rocks. In the contact zone, the rocks are mainly marble, dolomitic marble, hornfels, calcareous skarn, and magnesian skarn. The main ore-forming rock mass in this mine is granodiorite which was formed from collision and extrusion during Yanshanian. The Tongshan intrusion is mainly composed of quartz diorite, quartz monzonite porphyry, and granodiorite (Zhang et al., 2013, 2014). Granodiorite is most closely related to copper sulphide mineralization. The granodiorite yields a zircon LA-ICP-MS U-Pb age of 146.3 ± 3.2 Ma (Yu et al., 2014). SHRIMP zircon U-Pb dating indicated that the quartz monzonite porphyry was emplaced at 145.1 ± 1.2 Ma (Zhang et al., 2014). They are highly metamorphic and mineralized. Because of intruding into carbonate stratum, the mine mass had a strong contact metasomatism. The skarnization and hydrothermal alteration are always near the contact zone with silicification, pyritization, chloritization, carbonatation and potash feldspathization. The major ore types of the Tongshan copper deposit is Cu-bearing porphyries, Cu-bearing skarns, and Cu-bearing pyrites, among which the Cu-bearing skarns are related to the calc-alkaline porphyries (Gu et al., 2018). Major ore minerals include chalcopyrite, pyrite, magnetite, and pyrrhotite.

### 3. ANALYTICAL METHODS

#### 3.1. MAJOR AND TRACE ELEMENTS OF WHOLE ROCKS

Major elements and trace elements (including rare earth elements) were analyzed in ALS Laboratory Group - an Australian ICP-MS analytical lab in Guangzhou. For major element analysis, a calcined or ignited sample (~0.9 g) was added with lithium borate flux (~9.0 g, 50 % Li<sub>2</sub>B<sub>4</sub>O<sub>7</sub>-LiBO<sub>2</sub>), mixed well and fused in an auto fluxer at a temperature between 1050-1100 °C and then cooled to form a flat molten glass disc, and then analyzed by ME-XRF-06. Analytical

uncertainties were better than 1 %. Trace elements were analyzed by inductively coupled plasma-mass spectrometry (ICP-MS) of ME-MS81. The HNO<sub>3</sub> + HF seal dissolution method was used for trace elements and REE determination by adding Rh internal standard and converting the sample solutions into 1% HNO<sub>3</sub> medium. Rare earth elements were analyzed by cation exchange separation inductively coupled plasma atomic emission spectrometry (ICP-AES).

#### 3.2. MAJOR ELEMENTS OF BIOTITE

Major elements of biotite were determined by using a wavelength dispersive EPMA-1600 electron microprobe (EMP) at the Electron Microprobe Analysis Central, University of Science and Technology of China. The analysis was taken with an accelerating voltage of 15 kV, a low beam current (15 nA), and a defocused beam (5 μm). The calibration was based on a suite of mineral standards and oxide standards from the American standard committee.

## 4. RESULTS

### 4.1. ELEMENTAL ANALYSIS RESULTS

Major and trace element data for representative samples of the Tongshan intrusions are listed in Table 1. The Tongshan intrusion has a limited variation in SiO<sub>2</sub> content (64.1-65.7 wt.%). The K<sub>2</sub>O contents range from 3.24 to 3.82 wt.%, and total alkali concentrations are high (Na<sub>2</sub>O+K<sub>2</sub>O = 6.69-7.16 wt.%). The Fe<sub>2</sub>O<sub>3</sub> contents range from 4.36 to 5.22 wt.%, whereas Al<sub>2</sub>O<sub>3</sub> contents vary from 14.59 to 16.20 wt.%. In a plot of SiO<sub>2</sub> versus (Na<sub>2</sub>O+K<sub>2</sub>O) (Fig. 2a), the Tongshan intrusion belongs to granodiorite. And, in a plot SiO<sub>2</sub> versus K<sub>2</sub>O (Fig. 2b), Tongshan intrusion falls in the fields of high-K, cal-alkaline series. Besides, Al<sub>2</sub>O<sub>3</sub>, Fe<sub>2</sub>O<sub>3</sub><sup>T</sup>, CaO, MgO, P<sub>2</sub>O<sub>5</sub>, TiO<sub>2</sub> exhibit good negative correlation with SiO<sub>2</sub>, suggesting that fractional crystallization of ilmenite occurs during the formation of the pluton rocks.

The Tongshan intrusion is poor in ΣREE content, ranging from 81.5 to 147 ug/g (average = 101 ug/g). The LREE/HREE values vary from 10.5 to 11.9, while the La<sub>N</sub>/Yb<sub>N</sub> values are 14.2~20.1. The Tongshan intrusion is characterized by high Al<sub>2</sub>O<sub>3</sub>, Sr contents and Sr/Y value, and low Y, Yb contents, with similar geochemical characteristics of adakites (Fig. 3a; Defant and Drummond, 1990; Richards and Kerrich, 2007). According from chondrite-normalized REE patterns (Fig. 4a), Tongshan intrusion exhibits high degree of fractionation between LREEs and HREEs, and slightly positive Eu anomalies except samples of 03TS01 having slightly negative Eu anomalies, indicating the fractional crystallization of plagioclase is not obviously. The chondrite-normalized REE patterns of the Tongshan intrusion slant to right, showing a relative enriched LREEs, similarly to the distribution patterns of under crustal rocks. Spider diagram normalized to primitive mantle is shown in

**Table 1** Major element (wt.%) and trace element (ug/g) of the Tongshan intrusions.

Sample No.	03TS0	03TS-3	03TS-4	03TS-5-1	03TS-5-2	03TS-5-3	03TS-6	03TS-7	03TS08	03TS-9
SiO <sub>2</sub>	64.1	64.5	65.7	65.4	65.2	64.9	65.1	67.1	64.6	64.5
TiO <sub>2</sub>	0.54	0.5	0.48	0.47	0.48	0.48	0.51	0.44	0.50	0.50
Al <sub>2</sub> O <sub>3</sub>	16.2	15.5	14.6	14.8	14.6	15.0	15.3	14.1	15.4	15.6
Fe <sub>2</sub> O <sub>3</sub> <sup>T</sup>	4.57	5.03	5.22	5.04	5.08	5.01	5.18	3.62	5.03	4.36
MnO	0.04	0.04	0.04	0.04	0.04	0.04	0.04	0.03	0.05	0.04
MgO	1.47	1.44	1.54	1.5	1.61	1.52	1.53	1.02	1.49	1.55
CaO	3.60	3.29	2.83	2.95	2.71	3.11	2.81	2.25	3.50	3.18
Na <sub>2</sub> O	3.45	3.51	3.1	3.17	3.02	3.27	3.38	3.24	3.45	3.52
K <sub>2</sub> O	3.24	3.36	3.72	3.67	3.82	3.55	3.64	3.09	3.71	3.49
P <sub>2</sub> O <sub>5</sub>	0.18	0.18	0.15	0.15	0.15	0.16	0.17	0.04	0.17	0.17
SrO	0.07	0.06	0.06	0.06	0.06	0.06	0.06	0.05	0.06	0.06
BaO	0.09	0.08	0.09	0.08	0.08	0.09	0.09	0.04	0.09	0.09
LOI	2.05	1.97	1.99	2.65	2.47	2.01	1.76	3.00	1.73	2.26
Total	99.6	99.5	99.5	99.9	99.3	99.2	99.6	98.1	99.8	99.3
Ba	1020	780	860	770	810	890	880	400	880	830
Ce	72.8	44.8	36.2	39.8	35.8	45.7	41.1	14.1	51.8	49.2
Co	7.9	7.8	13	13.8	11.0	12.7	11.0	13.2	9.8	8.1
Cr	10	22	21	18	21	22	20	17	22	19
Cs	1.25	3.28	2.37	3.04	2.88	2.24	2.90	2.88	2.49	2.21
Cu	695	157	3900	4140	6570	3090	1625	>10000	1350	649
Dy	2.51	1.92	1.43	1.52	1.42	1.87	1.66	0.62	2.13	2.17
Er	1.42	1.02	0.77	0.8	0.75	0.96	0.86	0.35	1.13	1.13
Eu	1.09	0.95	0.84	0.83	0.81	0.99	0.90	0.45	1.06	1.04
Ga	23.	22.3	21.4	20.7	21.3	22.4	22.1	20.0	22.7	22.0
Gd	3.84	2.39	1.84	1.96	1.8	2.3	2.14	0.68	2.73	2.76
Hf	4.7	1.3	1.2	1.40	1.4	1.2	1.2	0.7	1.3	1.40
Ho	0.48	0.39	0.28	0.31	0.28	0.37	0.33	0.13	0.43	0.44
La	30.2	25.	22.2	21.1	21.90	22.9	22.2	8.0	26.5	23.0
Lu	0.21	0.17	0.13	0.14	0.13	0.16	0.14	0.06	0.17	0.17
Mo	<2	1.33	1.32	1.24	1.56	1.34	1.29	1.48	1.27	1.37
Nb	12.6	13.7	12.7	12.3	12.7	13.2	13.1	13.3	13.2	14.1
Nd	22.1	15.6	12	12.9	11.7	15.6	13.9	3.9	17.6	17.4
Ni	6.0	8.0	13.1	10.9	8.9	12.6	10.3	8.6	8.8	7.4
Pb	17.0	9.1	15.7	14.5	16.3	14.8	9.6	24.2	9.4	11.5
Pr	6.37	4.78	3.76	4.12	3.66	4.83	4.33	1.22	5.50	5.35
Rb	83.4	72.2	81.6	81.1	84.2	77.4	74.6	69.1	79.5	73.6
Sm	3.82	2.85	2.12	2.3	2.1	2.75	2.49	0.73	3.15	3.14
Sn	1.0	1.0	1.2	1.1	1.1	1.4	1.1	1.1	1.1	1.2
Sr	1045	563	531	490	504	578	579	499	611	598
Ta	1.00	1.11	1.05	1.02	1.06	1.07	1.12	1.14	1.08	1.12
Tb	0.50	0.38	0.29	0.31	0.28	0.37	0.35	0.11	0.44	0.43
Th	11.5	11.0	11.1	10.9	10.8	11.4	10.5	8.5	12.0	10.6
Tl	<0.50	0.30	0.35	0.42	0.44	0.32	0.34	0.49	0.31	0.42
Tm	0.21	0.16	0.12	0.12	0.12	0.15	0.14	0.05	0.17	0.17
U	2.4	1.9	2	1.9	1.9	2.3	1.8	0.6	2.3	1.6
V	71	65	64	57.	60	66	67	24	68	66
W	2.0	0.5	0.4	0.3	0.4	0.4	0.3	1.0	0.4	0.3
Y	12.4	11.9	8.8	9.7	9.0	11.2	10.1	4.0	13.6	12.7
Yb	1.37	1.05	0.82	0.82	0.78	0.99	0.90	0.37	1.13	1.16
Zn	57	45	48	47	44	49	45	47	50	48
Zr	175	36.2	33.5	40.8	41.7	33.9	34.0	21.3	34.6	38.5
∑REE	147	102	82.8	87	81.5	99.9	91.4	30.8	114.0	108.0
LREE	136	94	77.1	81.1	76.0	92.8	84.9	28.5	106.0	99.1
HREE	11.6	8.4	6.5	6.8	6.4	8.2	7.4	2.8	9.4	9.5
LREE/HREE	11.7	11.1	11.8	11.9	11.9	11.4	11.4	10.1	11.2	10.5
(La/Yb) <sub>N</sub>	15.8	17.1	19.4	18.5	20.1	16.6	17.7	15.5	16.8	14.2
δEu	0.87	1.11	1.3	1.2	1.27	1.20	1.19	1.95	1.11	1.08

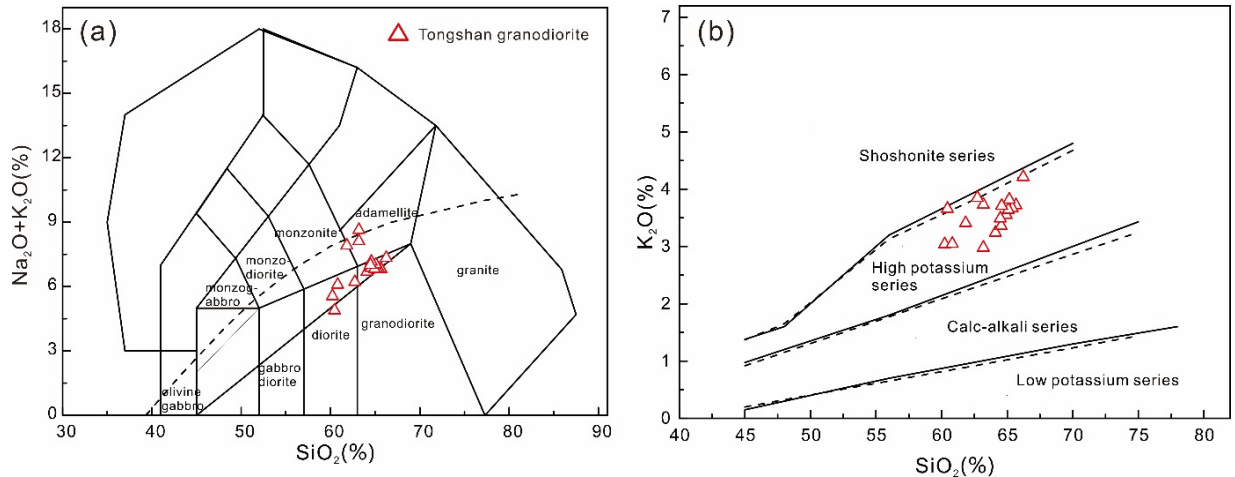


**Fig. 2** Geochemical characteristics of the Tongshan intrusion. (a)  $\text{SiO}_2$  vs.  $(\text{Na}_2\text{O} + \text{K}_2\text{O})$  diagram; (b)  $\text{SiO}_2$  vs.  $\text{K}_2\text{O}$  diagram.

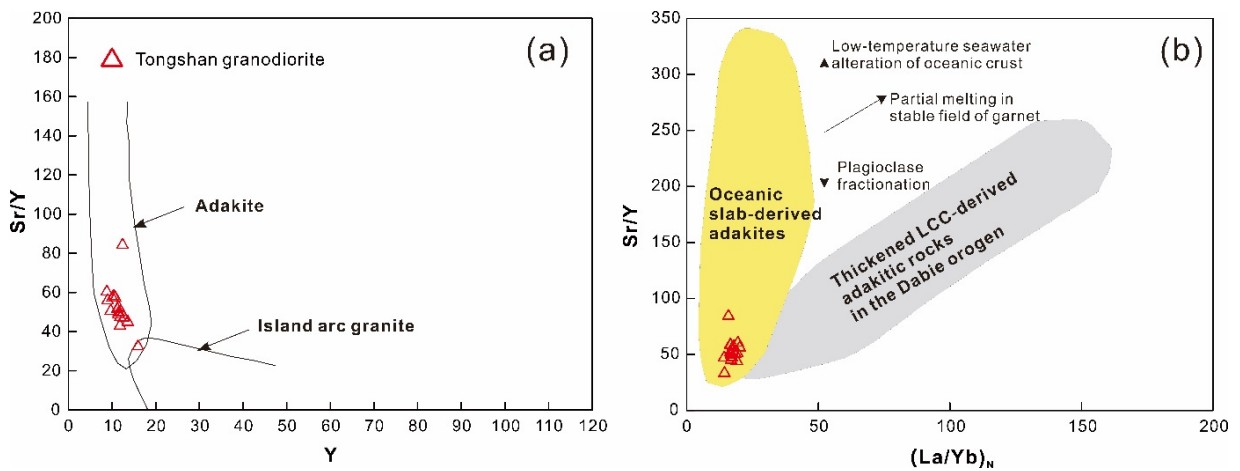


**Fig. 3** (a)  $\text{Sr}/\text{Y}$  vs.  $\text{Y}$  discrimination diagram of the Tongshan intrusion (from Liu et al. (2010)). (b)  $\text{Sr}/\text{Y}$  vs.  $(\text{La}/\text{Yb})_N$  diagram for adakites from the Tongshan. The data are from Guo et al. (2006).

Figure 4b. The Tongshan intrusion exhibits a depletion of large ion lithophile elements K, Sr, and enrichment of large ion lithophile elements Rb, Th, Nd.

#### 4.2. BIOTITE COMPOSITION

The major element chemistry of the biotite is listed in Table 2. Biotite  $\text{SiO}_2$  contents vary from 36.4 to 37.4 wt.%. The  $\text{MgO}$  contents range from 13.6 to 14.4 wt.% and are typical of values at the crust-mantle transition (Fig. 5). Biotite has low  $\text{Al}_2\text{O}_3$ ,  $\text{FeO}$  contents of 13.4–14.1 wt.%, 15.4–17.1 wt.%, respectively. The  $X_{\text{Mg}}$  values ( $\text{Mg}/(\text{Mg} + \text{Fe})$ ) for the biotite vary from 0.59 to 0.62, and such small variations suggest that these biotite grains are primary and they are magnesian (Defant et al., 1991).

### 5. DISCUSSION

#### 5.1. PETROGENESIS

The Tongshan intrusion is representative of intrusive rocks of the LYRB. Previous geochronological data, such as a K–Ar biotite (139 Ma) and Rb–Sr whole rock–single mineral isochron age (142 Ma) (Zhou et al., 2015), our

SHRIMP zircon U–Pb age of  $146.3 \pm 3.2$  Ma (Zhang et al., 2014), represents the formation age of the Tongshan intrusion in middle Yanshanian during the Late Jurassic (Gu et al., 2018). The ore bearing rock formed on 146–135 Ma has the adakitic features such as high Sr and low Yb in the LYRB (Zhou et al., 2015). The petrogenesis of the adakite is followed: (1) partial melting of the lower thickened crust and delamination partial melting of the lower crust and the mantle contamination (Jiang et al., 2010); (2) mixing of mantle derived magma and crustal magma (Wang et al., 2013; Shi et al., 2022); (3) the melt generated by particle melting of subducted oceanic crust mixed the enriched lithospheric mantle components (Ling et al., 2011; Sun et al., 2017; Liu et al., 2020); (4) the mantle derived magma by fractional crystallization or AFC process (Xie et al., 2018; Liang et al., 2018). The latest research shows that the chemical characteristics and genesis of adakitic rocks in the LYRB is consistent with subducted oceanic crust. Therefore, the LYRB (146–135 Ma) should belong to the subduction environment.

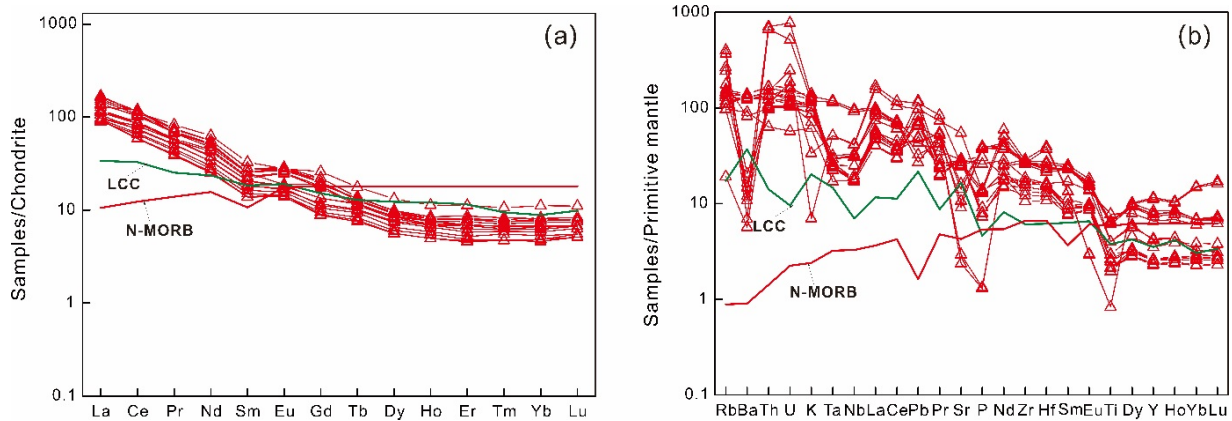


**Fig. 4** (a) Chondrite-normalized rare earth element patterns for the Tongshan intrusion. (b) Primitive mantle normalized trace element patterns for the Tongshan intrusion. The normalizing values are from Sun and McDonough (1989). LCC is from Rudnick and Gao (2013) and N-MORB is from Sun and McDonough (1989).

**Table 2** Major element of the biotite for the Tongshan intrusions (wt.%).

Sample No.	03TS06-1	03TS06-2	03TS06-3	03TS06-4	03TS06-5-1	03TS06-5-2	03TS06-6	03TS06-7	03TS06-8	03TS06-9-1
SiO <sub>2</sub>	35.9	36.9	37.0	37.2	37.2	36.8	36.1	36.9	36.8	36.8
TiO <sub>2</sub>	5.06	4.64	4.93	4.80	4.43	4.21	4.71	4.62	4.85	4.58
Al <sub>2</sub> O <sub>3</sub>	13.7	13.7	13.8	13.4	13.7	13.7	13.6	13.9	13.9	14.0
Fe <sub>2</sub> O <sub>3</sub>										
FeO	17.0	16.3	17.0	16.8	15.7	16.3	15.4	17.1	15.9	16.5
MnO	0.15	0.17	0.15	0.13	0.14	0.21	0.26	0.11	0.15	0.17
MgO	14.1	14.1	13.7	14	14.0	13.9	13.6	13.6	13.6	14.1
CaO	0	0	0	0	0	0	0	0	0	0
Na <sub>2</sub> O	0.20	0.21	0.19	0.19	0.13	0.15	0.20	0.20	0.21	0.15
K <sub>2</sub> O	9.36	9.26	9.53	9.16	9.06	9.41	9.54	9.24	9.65	9.76
H <sub>2</sub> O <sup>+</sup>										
F	0.41	0.42	0.32	0.24	0.22	0.32	0.19	0.27	0.26	0.30
Cl										
Si	5.42	5.54	5.52	5.58	5.62	5.57	5.53	5.55	5.54	5.51
Al <sup>IV</sup>	2.44	2.43	2.44	2.37	2.38	2.43	2.47	2.46	2.46	2.47
Al <sup>VI</sup>	0	0	0	0	0.05	0.01	0	0	0.02	0
Ti	0.57	0.52	0.55	0.54	0.50	0.48	0.54	0.52	0.55	0.52
Fe <sup>3+</sup>	0.38	0.46	0.43	0.46	0.50	0.42	0.39	0.45	0.43	0.38
Fe <sup>2+</sup>	1.77	1.58	1.70	1.65	1.49	1.65	1.59	1.70	1.58	1.68
Mn	0.02	0.02	0.02	0.02	0.02	0.03	0.03	0.01	0.02	0.02
Mg	3.17	3.15	3.05	3.12	3.16	3.14	3.12	3.04	3.06	3.14
Ca	0	0	0	0	0	0	0	0	0	0
Na	0.06	0.06	0.06	0.06	0.04	0.04	0.06	0.06	0.06	0.04
K	1.8	1.77	1.82	1.75	1.74	1.82	1.87	1.77	1.85	1.86
Total	15.62	15.54	15.57	15.54	15.50	15.58	15.61	15.55	15.57	15.62
Mg/(Mg+Fe)	0.59	0.61	0.59	0.60	0.61	0.60	0.61	0.59	0.60	0.60
P	85.76	82.93	84.86	64.98	84.94	87.61	94.68	92.01	96.53	96.62
H	2.83	2.74	2.80	2.15	2.8	2.89	3.12	3.04	3.19	3.19
T	770	762	765	764	759	751	768	757	767	759.

The Tongshan granodiorite has obviously adakitic signatures: such as high Sr (490–1045 ug/g), Na<sub>2</sub>O/K<sub>2</sub>O (0.83–1.06), low Y (4–13.6 ug/g), Yb (0.37–1.37 ug/g). These adakitic rocks are similar to LYRB adakite, which are derived from partial melting of the subducted oceanic crust towards LYRB during the early Cretaceous (Xie et al., 2018; Ling et al., 2011; Liu et al., 2010). Moreover, In Sr/Y vs. (La/Yb)<sub>N</sub> discrimination diagrams (Fig. 3b), Tongshan

granodiorite all falls in partial melting of the subducted oceanic crust area instead of LCC-derived adakitic rocks.

The Tongshan granodiorite zircon two-stage Hf model age is 1138 to 1422 Ma, which the two-stage Hf model age can represent the geological time of protolith separated from the depleted mantle (Gu et al., 2018). The two-stage Hf model age is like the exposed Proterozoic basement of southern Anhui age values

Table 2 continued

Sample No.	03TS06-9-2	03TS06-9-3	03TS06-10-1	03TS06-10-2	03TS06-11	03TS06-12	03TS06-13	03TS06-14	03TS06-15	03TS06-16
SiO <sub>2</sub>	36.4	37.1	37.1	37.0	37.6	36.7	36.4	37.3	37.0	37.1
TiO <sub>2</sub>	4.73	4.94	4.68	4.72	4.31	4.90	4.36	4.68	4.86	4.96
Al <sub>2</sub> O <sub>3</sub>	13.8	14.1	13.5	13.7	13.4	13.8	13.8	13.8	13.6	13.8
Fe <sub>2</sub> O <sub>3</sub>										
FeO	16.9	16.4	16.0	16.3	16.2	16.4	16.7	16.6	15.8	15.9
MnO	0.20	0.10	0.22	0.17	0.07	0.08	0.20	0.11	0.21	0.22
MgO	14.05	13.86	14.15	14.40	14.42	14.04	13.95	13.75	14.25	14.03
CaO	0	0	0	0	0	0	0	0	0	0
Na <sub>2</sub> O	0.18	0.13	0.19	0.12	0.13	0.16	0.20	0.18	0.19	0.30
K <sub>2</sub> O	9.25	9.80	9.29	8.59	9.28	9.08	9.55	9.55	9.27	9.62
H <sub>2</sub> O <sup>+</sup>										
F	0.12	0.29	0.28	0.28	0.19	0.38	0.28	0.24	0.27	0.30
Cl										
Si	5.49	5.53	5.58	5.55	5.64	5.52	5.51	5.58	5.55	5.54
Al <sup>IV</sup>	2.46	2.47	2.39	2.43	2.37	2.45	2.47	2.43	2.41	2.42
Al <sup>VI</sup>	0	0	0	0	0	0	0	0	0	0
Ti	0.54	0.55	0.53	0.53	0.49	0.56	0.50	0.53	0.55	0.56
Fe <sup>3+</sup>	0.37	0.43	0.45	0.53	0.44	0.48	0.36	0.44	0.45	0.42
Fe <sup>2+</sup>	1.76	1.61	1.56	1.52	1.59	1.58	1.75	1.64	1.53	1.57
Mn	0.03	0.01	0.03	0.02	0.01	0.01	0.03	0.01	0.03	0.03
Mg	3.16	3.07	3.17	3.22	3.22	3.15	3.15	3.07	3.19	3.12
Ca	0	0	0	0	0	0	0	0	0	0
Na	0.05	0.04	0.05	0.04	0.04	0.05	0.06	0.05	0.06	0.09
K	1.78	1.86	1.78	1.64	1.77	1.74	1.84	1.82	1.78	1.83
Total	15.60	15.6	15.5	15.5	15.6	15.5	15.6	15.6	15.6	15.6
Mg/(Mg+Fe)	0.60	0.60	0.61	0.61	0.61	0.60	0.60	0.60	0.62	0.61
P	91.7	93.9	70.6	82.0	63.7	88.6	94.7	82.9	78.3	80.1
H	3.03	3.10	2.33	2.71	2.10	2.92	3.13	2.74	2.59	2.64
T	763	767	765	765	755	769	754	760	770	770

(1200–1800 Ma) (Zhou et al., 2015), and the zircon  $\varepsilon_{\text{Hf}}(t)$  values is -7.64 to -2.08, with the average of -5.23 (Gu et al., 2018), illustrating that the Tongshan granodiorite could be derived from the crust mantle mixing magmatite provenance. The Sr isotope result shows that the  $(^{87}\text{Sr}/^{86}\text{Sr})_i$  value of Tongshan intrusions is ranging from 0.706737 to 0.707618 (Gu et al., 2018; Chen et al., 2014), indicating the source region of magma with crust mixing mantle. Therefore, the analysis below shows that the magma source of Tongshan intrusions is like the Tongling ore district (such as Tongguanshan rock) (Wang et al., 2022). Above all, we can speculate that the initial magma may be derived from the partial melting of the basement of southern Anhui and mixed with the mantle.

Furthermore, the Sr–Nd isotopic signatures of the intrusions in Guichi region plot toward the EM2 end member (Fig. 6a), and are like those of early Cretaceous mafic igneous rocks in the LYRB, which are formed by melting of lithospheric mantle and then metasomatized by subducted slab-derived melts/fluids (Wang et al., 2022; Sun et al., 2017; Liu et al., 2020). In the  $\varepsilon_{\text{Hf}}(t)$  versus age diagrams (Fig. 6b), the magmatic zircons displace upper the Paleo-Proterozoic crustal evolution line, while the inherited zircons plot upper the Archean line. Since Hf isotopes could be greatly enriched during magmatic evolution, Guichi intrusions might have been

assimilated by ancient crustal materials such as ancient metamorphic rocks. The source of the inherited zircons could be the Archean Kongling group and Paleoproterozoic Dongling group basement rocks (Wu et al., 2012; Xie et al., 2018). Therefore, the Tongshan intrusion could be formed by the partial melting of subducted oceanic slab according to the geochemical and compiled Sr–Nd isotope data.

## 5.2. TECTONIC IMPLICATIONS

The tectonic setting of Mesozoic magma and mineralization in the LYRB has great dispute. Some think that the area of Mesozoic in extensional background, has nothing to do with the subduction of the paleo-Pacific Ocean, and may be thickened crust and continental sedimentation in extensional environment (Wang et al., 2013; Ling et al., 2011). Sun et al. (2017) consider that the LYRB in the early Cretaceous was formed by the ridge subduction between Izanagi plate and the Pacific plate through a comprehensive study of magmatic rocks, sedimentary basin, tectonic of the area (Wang et al., 2015). Liu et al. (2020) considers that the adakite of the LYRB is mainly related to the ocean subduction through the geochemical characteristics of the ore bearing adakite of the LYRB in contrast to the ore barren adakite of the southern part of the Tanlu fault (Liu et al., 2010, 2020). The paleo-Pacific plate subduction system opinion is on the basis of the

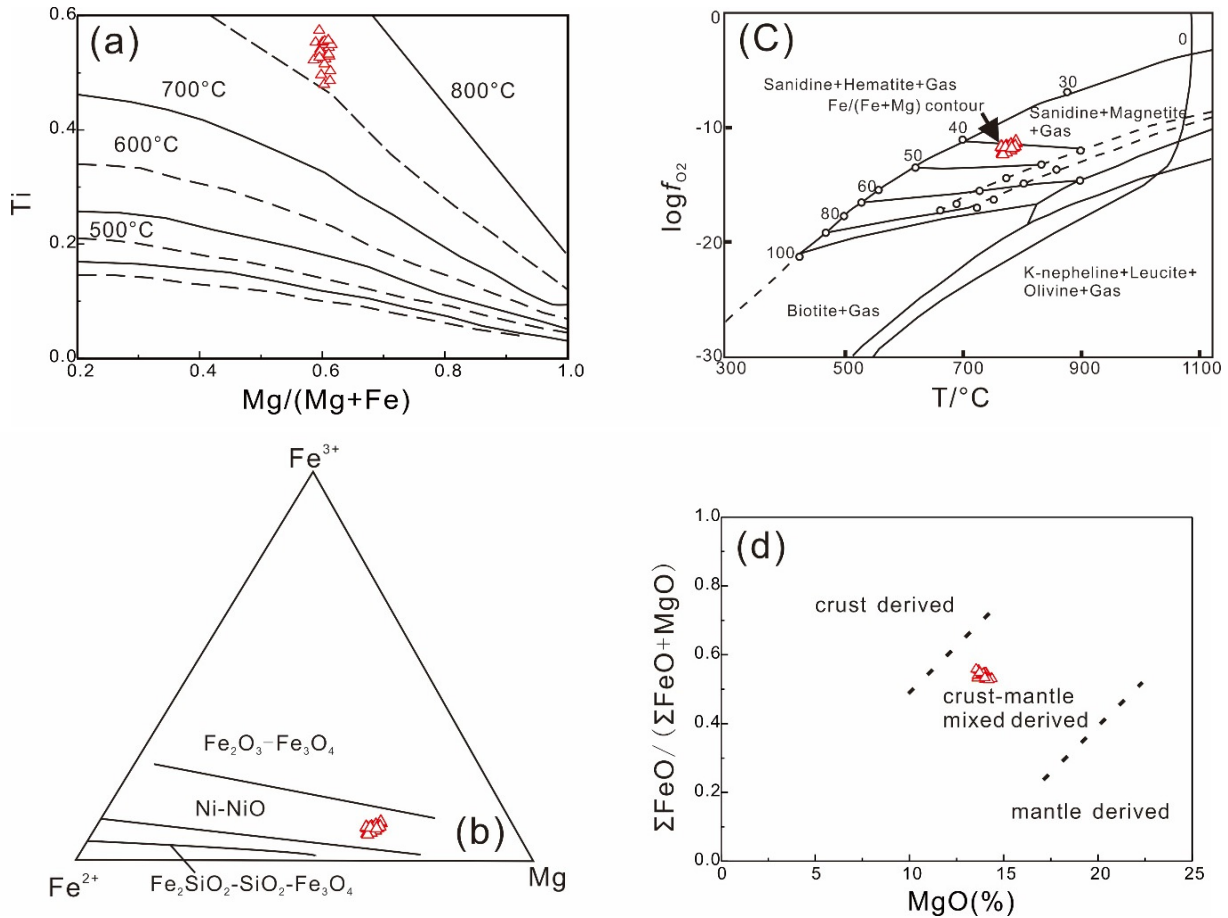


Fig. 5 Discrimination diagrams for biotite (from Defant et al. (1991)).

temporal spatial distribution and geochemical characteristics of magmatite, proposed that the Yanshanian magmatism in the LYRB could be closely related to subduction of the paleo-Pacific plate, which the early ore bearing rock is formed in a continental margin environment, while the late shoshonite series magmatite, Shuangfeng volcano rock and A-type granites are formed in extensional environment (Xie et al., 2018; Yang et al., 2016). This model can well explain the temporal spatial distribution and geochemical characteristics of the early ore bearing adakitic rocks and the later shoshonite series of magmatite, Shuangfeng volcano rock as well as A-type granite.

The Tongshan intrusions fall into the volcanic arc granite (VAG) and syn-collision granite (Syn-COLG) fields, indicating that the Tongshan intrusion is generated in an arc setting. Furthermore, the zircon emplacement age temporally coincides with the compressional to extensional transition in the LYRB. In summary, integrated with the geochronology and geochemical results for the Guichi intrusion, this is arc magmatism related to subduction of oceanic crust in a continental margin setting, considering that the Tongshan intrusion may be derived from the partial melting of subducted oceanic slab.

### 5.3. TEMPERATURE, OXYGEN FUGACITY AND PETROGENESIS

Since the Ti content in biotite is a critical control factor of the crystallization temperature (Zhang et al., 2013b), the Ti concentration of biotite could be used as a biotite geothermometer. According to the empirical formula provided by Henry et al. (2005), the crystallization temperature of Tongshan intrusion is ranging from 750 °C to 770 °C, suggesting a relatively higher temperature of the intrusive magma. The calculated temperature based on biotite geothermometer is consistent with the result inferred from the Ti–Mg/(Mg + Fe) diagram (Fig. 5a).

The total cations of Al in biotite is positively correlated with the consolidation pressure of granite (Defant et al., 1991), following the equation as:  $P(100 \text{ MPa}) = 3.03T_{\text{Al}} - 6.53(\pm 0.33)$ . The  $T_{\text{Al}}$  is the total cations of Al in biotite, which is assumed with 22 oxygen atoms. The crystallization pressure of biotite in Tongshan intrusion is in the range of 63–96 MPa, equivalent to a depth of 2.1–3.2 km.

The oxidation condition during the magma crystallization also can be reflect from the chemical composition of biotite. The magmatic oxygen fugacity can be calculated by the concentrations of  $\text{Fe}^{3+}$ ,  $\text{Fe}^{2+}$ , and  $\text{Mg}^{2+}$  in biotite, which is paragenetic with K-feldspar and magnetite (Wones and Eugeter, 1965).

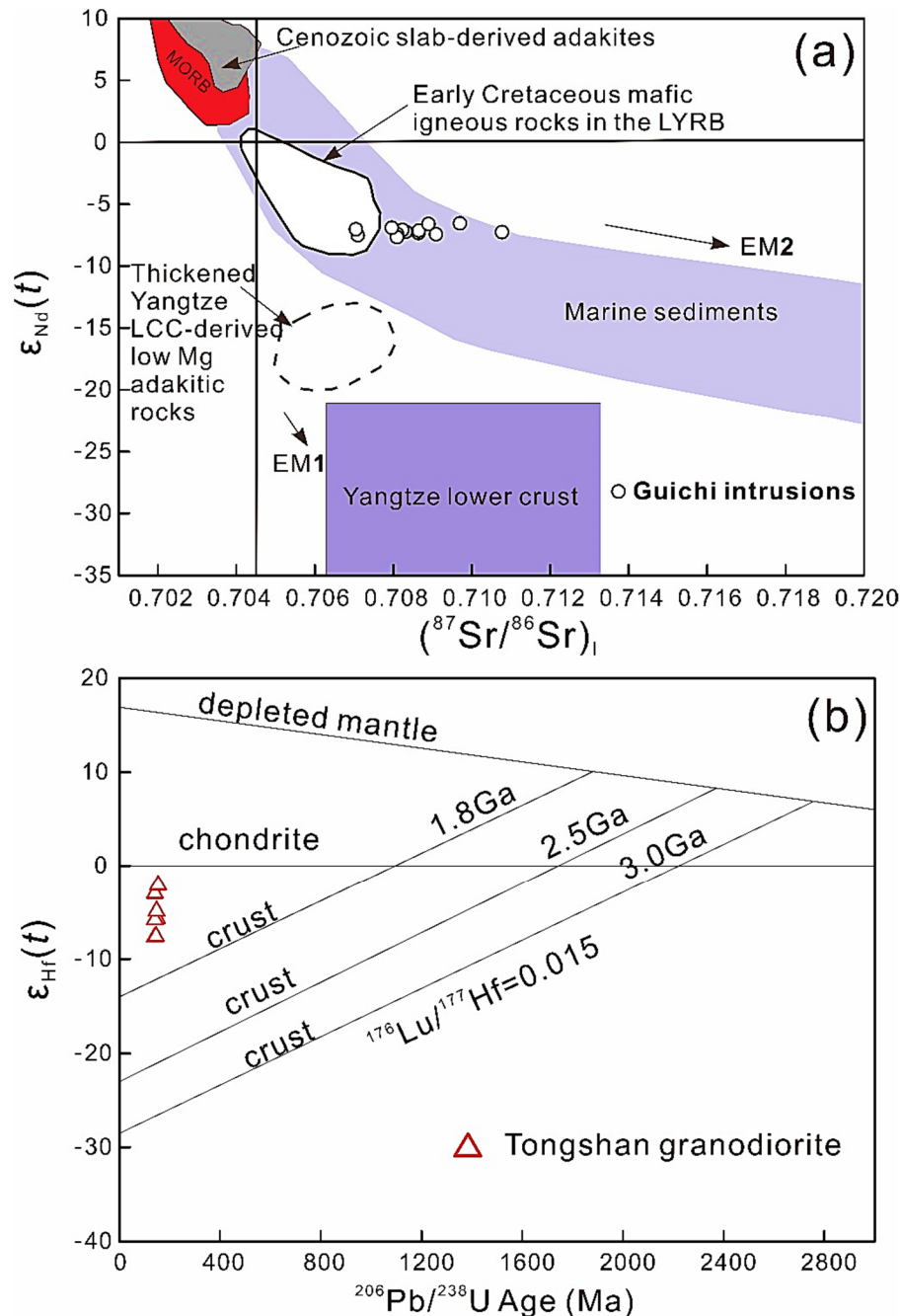


**Fig. 6** (a) Sr–Nd isotopes of the Tongshan intrusions. (b)  $\epsilon_{Hf}(t)$  vs. U–Pb age diagram of zircons in Tongshan intrusion. The data sources are from Gu et al. (2018). Slab melts are represented by Cenozoic adakites (Liu et al. 2010). UCC is represented by the Neoproterozoic Shangxi Group, south Anhui province with volcanic sediments, low grade metamorphic phyllite rocks, sandstone, limestone, and shale (Wang et al., 2010). LCC of the Yangtze block is represented by the Kongling TTG gneisses (Jahn et al., 1999). LYRB represents the Lower Yangtze River Metallogenic Belt.

The biotite from Tongshan intrusion is plotted between Ni–NiO buffer line and  $Fe_2O_3$ – $Fe_3O_4$  buffer line in the  $Fe^{3+}$ – $Fe^{2+}$ –Mg diagram (Fig. 5b), indicating that the crystallization of biotite may be associated with a high oxygen fugacity (Wones and Eugeter, 1965). The magmatic oxygen fugacity balanced with the biotite + sanidine + magnetite can be evaluated from the  $\log(fO_2)$ – $T$  diagram (Wong et al., 2009). Therefore, the oxygen fugacity of the biotite is estimated to be  $10^{-11}$  to  $10^{-13}$  bars (Fig. 5c), indicating

the biotite of the Tongshan intrusion may be formed in a moderate oxidation condition during magma crystallization. High oxygen fugacity may remove sulphide in the source region and make the melt sulphide under-saturated, thereby promoting porphyry copper mineralization (Sun et al., 2015, 2017). Meanwhile, high oxygen fugacity can extract additional sulphur in the form of sulphate during partial melting, liberating more chalcophile elements, which are consequently scavenged by magmatic fluids

when the oxygen fugacity is reduced (Sun et al., 2017; Liu et al., 2020). Therefore, high oxygen fugacity can transform more sulphide to sulphate, which induces sulphur-undersaturated magmas and consequently allows assimilation of more sulphide (Sun et al., 2015, 2017). Copper is incompatible in sulphur-undersaturated magmas; when initial concentration of copper is high in oxidized magmas (Sun et al., 2015, 2017; Zhang et al., 2013b), conditions are favourable for copper mineralization.

Meanwhile, the magmatic material source can be also reflected by the composition of biotite (Wang et al., 2015). The FeO/(FeO + MgO) vs. MgO diagram (Fig. 5d) shows the Tongshan granodiorite was derived from crust–mantle mixed source. Most of the hydrothermal–magmatic Cu–Au deposits are great closely related with the calc-alkaline intrusions which have high oxygen fugacity (Sun et al., 2015, 2017).

## 6. CONCLUSIONS

Elemental data and major elements of biotite of the Tongshan intrusion, integrated with a comprehensive study of Sr–Nd–Hf isotopes, zircon U–Pb geochronology and major and trace element geochemistry of the Late Mesozoic intrusion in the Guichi region leads to the following conclusions:

(1) Elemental geochemical, and Sr–Nd isotopic data show that the Tongshan intrusion was most likely formed by the partial melting of subducted oceanic crust, mixed with the enriched lithospheric mantle components.

(5) The Tongshan magmatite assemblages and geochemical characteristics change with time is consistent with the overall variation characteristic of magmatite in the LYRB, and it displays the contemporary adakites formed in the tectonic setting of the same, namely the paleo-Pacific subduction. Therefore, Tongshan metallogenic district, even the whole LYRB is associated with the paleo-Pacific subduction, and the high oxygen fugacity is the key feature of mineralization.

## ACKNOWLEDGEMENTS

This work is supported by the National Natural Science Foundation of Hunan Province (Grant No. 2022JJ50063, 2020JJ5139), the Social and Science Fund of Hunan Province (Grant No. 18JD26) and the General Project of Department of education of Hunan Province (Grant No. 20C0623, 20C0647).

## REFERENCES

- Chang, Y.F., Liu, X.P. and Wu, Y.C.: 1991, The Copper–Iron belt of the lower and middle reaches of the Changjiang River. Geological Publishing House, Beijing, 1–238, (in Chinese).
- Chen, L., Zhao, Z.F. and Zheng, Y.F.: 2014, Origin of andesitic rocks: geochemical constraints from Mesozoic volcanics in the Luzong basin, South China. *Lithos*, 190, 220–239. DOI: 10.1016/j.lithos.2013.12.011
- Defant, M.J., Richerson, P.M., DeBoer, J.Z. et al.: 1991, Dacite genesis via both slab melting and differentiation: petrogenesis of La Yegueda volcanic complex, Panama. *J. Petrol.*, 32, 1101–1142. DOI: 10.1093/petrology/32.6.1101
- Defant, M.J. and Drummond, M.S.: 1990, Derivation of some modern arc magmas by melting of young subduction lithosphere. *Nature*, 347, 662–665. DOI: 10.1038/347662a0
- Deng, J.H., Yang, X.Y., Li, S. et al.: 2016, Partial melting of subducted paleo-Pacific plate during the early Cretaceous: constraint from adakitic rocks in the Shaxi porphyry Cu–Au deposit, Lower Yangtze River Belt. *Lithos*, 262, 651–667. DOI: 10.1016/j.lithos.2016.07.039
- Gilder, S.A., Keller, G.R. and Luo, M.: 1991, Eastern Asia and the western Pacific timing and spatial distribution of rifting in China. *Tectonophysics*, 197, 225–243. DOI: 10.1016/0040-1951(91)90043-R
- Gu, H.L., Yang, X.Y., Nie, Z.X. et al.: 2018, Study of late-Mesozoic magmatic rocks and their related copper–gold–polymetallic deposits in the Guichi ore-cluster district, Lower Yangtze River Metallogenic Belt, East China. *Int. Geol. Rev.*, 60, 1404–1434. DOI: 10.1080/00206814.2017.1422442
- Guo, F., Fan, W.M. and Li, C.W.: 2006, Geochemistry of late Mesozoic adakites from the Sulu belt, eastern China: magma genesis and implications for crustal recycling beneath continental collisional orogens. *Geol. Mag.*, 143, 1–13. DOI: 10.1017/S0016756805001214
- Henry, D.J., Guidotti, C.V. and Thomsen, J.A.: 2005, The Ti-saturation surface for low-to medium pressure metapelitic biotites: implications for geothermometry and Ti-substitution mechanisms. *Am. Mineral.*, 90, 316–328. DOI: 10.2138/am.2005.1498
- Hu, L., Du, Y.S., Wang, A.J. et al.: 2017, Adakitic rocks explained by the deep accumulation of amphibole and apatite near the crust–mantle boundary: a case study from the Tongling region, Lower Yangtze River belt, eastern China. *Geochem. J.*, 51, 551–569. DOI: 10.2343/geochemj.2.0491
- Jiang, Y.H., Zhao, P., Zhou, Q. et al.: 2010, Petrogenesis and tectonic implications of Early Cretaceous S- and A-type granites in the northwest of the Gan–Hang rift, SE China. *Lithos*, 121, 55–73. DOI: 10.1016/j.lithos.2010.10.001
- Jahn, B.M., Wu, F.Y., Lo, C.H. et al.: 1999, Crust–Mantle interaction induced by deep subduction of the continental crust: Geochemical and Sr–Nd isotopic evidence from post-collisional mafic–ultramafic intrusions of the northern Dabie complex, central China. *Chem. Geol.*, 157, 119–146. DOI: 10.1016/S0009-2541(98)00197-1
- Liang, S.N., Wei, J.H., Zhao, Z.X. et al.: 2018, The Cretaceous Huangdaoshan Cu-bearing intrusion in Chuzhou: Petrogenesis and implications for the Cu mineralization in the Middle–Lower Yangtze River Valley Metallogenic Belt, eastern China. *Ore Geol. Rev.*, 101, 900–918. DOI: 10.1016/j.oregeorev.2018.08.022
- Ling, M.X., Wang, F.Y., Ding, X. et al.: 2011, Different origins of adakites from the Dabie Mountains and the Lower Yangtze River belt in eastern China: geochemical constraints. *Int. Geol. Rev.*, 53, 727–740. DOI: 10.1080/00206814.2010.482349
- Liu, S.A., Li, S., He, Y. et al.: 2010, Geochemical contrasts between early Cretaceous ore-bearing and ore-barren high-Mg adakites in central-eastern China: implications for petrogenesis and Cu–Au

- mineralization. *Geochim. Cosmochim. Acta*, 74, 7160–7178. DOI: 10.1016/j.gca.2010.09.003
- Liu, H., Liao, R.Q., Zhang, L.P. et al.: 2020, Plate subduction, oxygen fugacity, and mineralization. *J. Oceanol. Limnol.*, 38, 1, 64–74. DOI: 10.1007/s00343-019-8339-y
- Mao, J.W., Xie, G.Q., Duan, C. et al.: 2011, A tectonogenetic model for porphyry-skarn-strata bound Cu–Au–Mo–Fe and magnetite–apatite deposits along the Middle-Lower Yangtze River Valley, Eastern China. *Ore Geol. Rev.*, 43, 294–314. DOI: 10.1016/j.oregeorev.2011.07.01
- Richards, J.P. and Kerrich, R.: 2007, Special paper: Adakite-like rocks: Their diverse origins and questionable role in metallogenesis. *Econ. Geol.*, 102, 537–576. DOI: 10.2113/gsecongeo.102.4.537
- Rudnick, R.L. and Gao, S.: 2003, Composition of the continental crust. In: Rudnick, R.L., Holland, H.D. and Turekian, K.K. (eds.), *Treatise on Geochemistry*, vol. 3, The Crust. Elsevier-Perгамon, Oxford, 1-64.
- Shi, Y., Tang, Y.L., Li, X. et al.: 2022, Mesozoic tectonic transition from the Tethyan to Paleo-Pacific domains in South China: New insights from Mesozoic igneous rocks in the western Nanling Range. *J. Asian Earth Sci.*, 239, 105406, DOI: 10.1016/j.jseae.2022.105406
- Sun, W.D., Huang, R.F., Li, H., et al.: 2015, Porphyry deposits and oxidized magmas. *Ore Geol. Rev.*, 65, 97–131. DOI: 10.1016/j.oregeorev.2014.09.004
- Sun, W.D., Wang, J.T., Zhang, L.P. et al.: 2017, The formation of porphyry copper deposits. *Acta Geochim.*, 36, 1, 9–15. DOI: 10.1007/s11631-016-0132-4
- Sun, S.S. and McDonough, W.: 1989, Chemical and isotopic systematic of oceanic basalt: Implication for mantle composition and processes. In: Saunders, A.D. and Norry, M.J. (eds.), *Magmatism in the ocean basins*. *Geol. Soc. Spec. Publ.*, 42, 313–345. DOI: 10.1144/GSL.SP.1989.042.01.19
- Wang, Y., Yang, X.Y., Deng, J.H. et al.: 2022, A comprehensive overview on the origin of intrusive rocks and polymetallic mineralization in the Tongling ore-cluster region, lower Yangtze River Metallogenic Belt: Geological and geochemical constraints. *Ore Geol. Rev.*, 141, 104625. DOI: 10.1016/j.oregeorev.2021.104625
- Wang, M.F., Zhao, R.Z., Shang, X.Y. et al.: 2020, Factors controlling Pt–Pd enrichments in intracontinental extensional environment: Implications from Tongshankou deposit in the Middle–Lower Yangtze River Metallogenic Belt, Eastern China. *Ore Geol. Rev.*, 124, 103621. DOI: 10.1016/j.oregeorev.2020.103621
- Wang, S.W., Zhou, T.F., Yuan, F. et al.: 2015, Geological and geochemical studies of the Shujiadian porphyry Cu deposit, Anhui Province, Eastern China: Implications for ore genesis. *J. Asian Earth Sci.*, 103, 252–275. DOI: 10.1016/j.jseae.2014.08.004
- Wang, F.Y., Liu, S.A., Li, S.G. et al.: 2013, Contrasting zircon Hf–O isotopes and trace elements between ore-bearing and ore-barren adakitic rocks in central-eastern China: implications for genetic relation to Cu–Au mineralization. *Lithos*, 156–159, 97–111. DOI: 10.1016/j.lithos.2012.10.017
- Wang, L.J., Griffin, W.L., Yu, J.H. et al.: 2010, Precambrian crustal evolution of the Yangtze Block tracked by detrital zircons from Neoproterozoic sedimentary rocks. *Precambrian Res.*, 177, 131–144. DOI: 10.1016/j.precamres.2009.11.008
- Wones, D.P. and Eugeter, H.P.: 1965, Stability of biotite: experiment, theory, and application. *Am. Mineral.*, 50, 1228–1272.
- Wong, J., Sun, M., Xing, G.F. et al.: 2009, Geochemical and zircon U–Pb and Hf isotopic study of the Baijhuajian metaluminous A-type granite: Extension at 125~100Ma and its tectonic significance for South China. *Lithos*, 112, 289–305. DOI: 10.1016/j.lithos.2009.03.009
- Wu, F.Y., Ji, W.Q., Sun, D.H. et al.: 2012, Zircon U–Pb geochronology and Hf isotopic compositions of the Mesozoic granites in southern Anhui Province, China. *Lithos*, 150, 37–48. DOI: 10.1016/j.lithos.2012.03.020
- Xie, J.C., Wang, Y., Li, Q.Z. et al.: 2018, Early Cretaceous adakitic rocks in the Anqing region, southeastern China: constraints on petrogenesis and metallogenic significance. *Int. Geol. Rev.*, 60, 1435–1452. DOI: 10.1080/00206814.2017.1362672
- Xu, Y.M., Jiang, S.Y. and Zhu, J.X.: 2021, Factors controlling the formation of large porphyry Cu deposits: A case study from the Jiurui ore district of Middle-Lower Yangtze River Metallogenic Belt using in situ zircon and apatite chemistry from syn-mineralization intrusions. *Ore Geol. Rev.*, 133, 104082. DOI: 10.1016/j.oregeorev.2021.104082
- Yang, Y.Z., Wang, Y., Ye, R.S. et al.: 2016, Petrology and geochemistry of Early Cretaceous A-type granitoids and late Mesozoic mafic dikes and their relationship to adakitic intrusions in the lower Yangtze River belt, Southeast China. *Int. Geol. Rev.*, 59, 62–79. DOI: 10.1080/00206814.2016.1212284
- Yang, X.Y. and Lee, I.: 2011, Review of the stable isotope geochemistry of Mesozoic igneous rocks and Cu–Au deposits along the middle–lower Yangtze metallogenic belt, China. *Int. Geol. Rev.*, 53, 741–757. DOI: 10.1080/00206814.2010.533881
- Yu, L.F., Nihemaiti, M., Gu, H.L. et al.: 2014, Zircon U–Pb geochronology and Hf isotopic geochemistry of the Tongshan Cu(Au) deposit in Anhui. *J. Earth Sci. Environ.*, 36, 1, 152–160, (in Chinese with English abstract).
- Zhang, Z.Y., Du, Y.S., Teng, C.Y. et al.: 2014, Petrogenesis, geochronology, and tectonic significance of granitoids in the Tongshan intrusion, Anhui Province, Middle-Lower Yangtze River Valley, eastern China. *J. Asian Earth Sci.*, 79, 792–809. DOI: 10.1016/j.jseae.2013.04.007
- Zhang, Z.Y., Du, Y.S. and Zhang, J.: 2013a, Alteration, mineralization, and genesis of the zoned Tongshan skarn-type copper deposit, Anhui, China. *Ore Geol. Rev.*, 53, 489–503. DOI: 10.1016/j.oregeorev.2013.02.009
- Zhang, H., Ling, M.X., Liu, Y.L. et al.: 2013b, High oxygen fugacity and slab melting Linked to Cu mineralization: Evidence from Dexing porphyry copper deposits, Southeastern China. *J. Geol.*, 121, 289–305. DOI: 10.1086/669975
- Zhou, T.F., Wang, S.F., Fan, Y. et al.: 2015, A review of the intracontinental porphyry deposits in the Middle-Lower Yangtze River Valley metallogenic belt, Eastern China. *Ore Geol. Rev.*, 65, 433–456. DOI: 10.1016/j.oregeorev.2014.10.002